Preparation of NiW/Ti-USY Catalyst and Its Hydrodeoxygenation Performance in Biomass Oil

Mingyuan Gao, a Jin Li, a,* Jiao Jiang, and Tao Pan b

A catalyst (NiW/Ti-USY) was prepared *via* an impregnation method. Its catalytic performance was investigated for the hydrodeoxygenation (HDO) of Jatropha oil. It was found that the support composition significantly influenced the Lewis acid site concentration, thereby affecting the deoxygenation performance. The catalyst exhibited optimal activity when the Ti loading reached 9 wt%. Furthermore, under the same support conditions, a Ni/W mass ratio of 1:9 and a total NiW loading of 30% resulted in the best catalytic performance, achieving a deoxygenation rate exceeding 90% and a minimum olefin content of 9.64%. GC-MS analysis of the product oil revealed a ratio of $(C_{15} + C_{17})/(C_{16} + C_{18})$ greater than 10, indicating that the decarbonylation/decarboxylation (DCO/DCO₂) pathway dominated the hydrodeoxygenation process.

DOI: 10.15376/biores.20.4.10552-10567

Keywords: Hydrogenation deoxygenation; NiW; Ti-USY; Jatropha oil; Acid sites; Deoxygenation degree; Decarbonylation/decarboxylation ratio

Contact information: a: School of Chemistry and Chemical Engineering, Hainan University, Haikou 570228, China; b: Hainan Institute of Industry, Haikou 570100, China;

* Corresponding author: 316800681@gg.com

INTRODUCTION

Against the backdrop of rapid social and industrial development, global demand for fossil fuels continues to grow. However, their excessive use has triggered severe environmental issues, including greenhouse gas emissions and climate change. Therefore, developing and promoting green and sustainable alternative energy sources has become an urgent task. Biomass resources, particularly non-edible oils such as Jatropha oil, have attracted widespread attention in recent years as renewable feedstocks for producing alternative fuels (Zhong *et al.* 2023). Nevertheless, natural biomass oils contain high levels of fatty acids and suffer from issues such as high oxygen content (>40%), low calorific value (approximately 30 to 40 MJ/kg), high olefin content, and poor chemical stability, which severely limit their direct application (Zhang *et al.* 2022). Effectively upgrading the quality of biomass oil is key to realizing its high-value utilization (Liu *et al.* 2023).

Catalytic hydrodeoxygenation (HDO) technology is one of the most effective pathways for biomass oil upgrading, with its core lying in the design of high-performance catalysts (Fang *et al.* 2024). The ultimate goal of this study is to convert Jatropha oil into clean diesel fuel (C₁₅ to C₁₈ alkanes) that meets international standards through the development of an efficient NiW/Ti-USY catalyst system. Unlike biodiesel (FAME) produced *via* traditional transesterification, this research aims to produce second-generation biodiesel (green diesel), whose chemical composition is identical to petroleum-based diesel. It can be directly used in existing diesel engines without any modifications (Knothe 2022). Utilizing sustainable biomass resources to produce green diesel is of great

significance for reducing dependence on fossil fuels (Wang and Chen 2024).

To achieve this goal, an ideal HDO catalyst must possess excellent deoxygenation activity, high hydrothermal stability, and outstanding anti-coking ability to ensure long catalytic life (Liu and Yang 2023). Although noble metal catalysts (Pt, Pd) exhibit high activity, their high cost hinders large-scale industrial application (Chen and Li 2023). Therefore, developing efficient and stable catalysts based on non-noble metals (e.g., Ni, W, Mo) has become a mainstream research direction (Xu and Cheng 2024).

Among non-noble metal catalysts, NiW-based catalysts have attracted significant attention due to their unique hydrodeoxygenation performance and potential synergistic effects (Wang et al. 2023). Studies have shown that bimetallic catalysts demonstrate higher catalytic activity due to the addition of a second metal (Fang et al. 2024). For instance, Ni-Mo/SiO₂ catalysts achieved a 93.5% conversion rate and an 89.6% molar yield of C15-C18 alkanes from Jatropha oil (Xu and Cheng 2024). However, catalyst performance heavily depends on the support properties. Zeolite supports (USY) are widely used in HDO reactions due to their excellent cracking and isomerization capabilities. In recent years, researchers have attempted to modify USY by introducing secondary components (Ti, Ce, Er) to adjust its acidity and pore structure, thereby improving metal dispersion, enhancing metal-support interactions, and ultimately boosting HDO performance. Developing novel catalyst support materials is an important research direction for improving HDO efficiency (Li et al. 2024).

Despite some progress, existing research still faces several unresolved issues: studies specifically targeting biomass oil HDO are relatively limited; the optimal threshold effect and synergistic mechanism of Ti-modified USY supports remain unclear; and research on catalyst long-term stability, anti-poisoning ability, and regeneration performance is insufficient (García-Mendoza *et al.* 2023). Particularly, catalyst fouling and deactivation mechanisms during prolonged operation represent a core challenge hindering industrialization (Liu and Yang 2024). In-depth investigation into catalyst deactivation mechanisms is crucial for developing long-lasting and stable industrial catalysts.

Based on the current research landscape and technical challenges, the innovation of this study lies in the systematic optimization of Ti modification levels, NiW loading, and metal ratios, leading to the successful development of a high-performance NiW/Ti-USY catalyst system. This system achieves deep deoxygenation while obtaining highly selective C₁₅-C₁₇ alkane products, providing critical technical support for the industrial application of green diesel production from biomass oils.

EXPERIMENTAL

Materials

Ni nitrate [Ni (NO₃) 2 6H₂O] (98%) was purchased from Xilong Science Co., Ltd. Ammonium metastungstate hydrate (99.5%) and titanium sulfate (96%) were purchased from Shanghai McBiochemical Technology Co., Ltd. The USY catalyst (SiO₂/Al₂O₃: 5.4) was purchased from Nankai District, Tianjin. Nitrogen 99.999% and hydrogen 99.999% were from Haikou Huateng Chemical Gas Co., Ltd. Dichloromethane (99.5%) was purchased from Xilong Science Co., Ltd.

Synthesis of the Catalyst

The Ti-USY supported NiW catalyst was prepared by the following procedure. First, a certain amount of Ti(SO₄)₂ was dissolved in 200 mL of ultrapure water together with 4.0 g of USY zeolite. The mixture was stirred at 80 °C for 2 h, then separated by centrifugation. The solid was collected and dried at 110 °C for 2 h. The resulting powder was further calcined at 500 °C for 3 h with a heating rate of 10 °C/min to obtain the Timodified USY support. Subsequently, an aqueous solution was prepared by dissolving Ni(NO₃)₂·6H₂O and (NH₄)₆H₂W₁₂O₄₀·xH₂O in deionized water. Then, 2.0 g of the Ti-USY support was added to this solution, and the mixture was stirred at 80 °C for 6 h. After impregnation, the sample was dried at 105 °C overnight. The dried solid was then calcined at 400 °C for 4 h in a muffle furnace with a heating rate of 10 °C/min. Finally, the catalyst was reduced under H₂ atmosphere at 350 °C for 2 h to obtain the final NiW/Ti-USY catalyst.

Catalyst Characterization

The catalyst was characterized using multiple techniques under the following conditions: X-ray diffraction (XRD) was performed using a 3 kW source with a scanning range of 5° to 80° at a speed of 10°/min. Scanning electron microscopy (SEM) was conducted at an accelerating voltage of 10 kV. Transmission electron microscopy (TEM) was carried out at 200 kV with a point resolution of 0.14 nm. The specific surface area and pore structure were determined by N₂ physisorption using the Brunauer–Emmett–Teller (BET) method at 473 K. Pyridine-adsorption infrared spectroscopy (Py-IR) measurements involved pre-treating the sample under vacuum at 350 °C for 2 h, followed by pyridine adsorption at room temperature for 30 min. After acquiring the adsorption spectrum, the sample was heated to 150 and 350 °C at a rate of 10 °C/min to obtain total acid and strong acid spectra, respectively. X-ray photoelectron spectroscopy (XPS) was performed using an Al K α radiation source (1486.8 eV), with a spot size of 50 to 400 μ m, an operating voltage of 15 kV, and a current of 10 mA. Data were collected with a step size of 0.05 eV and 1–15 scans per region.

Catalytic Hydrodeoxygenation and Product Analysis

The experiment was conducted in an intermittent high-pressure reactor, and 10 g of jatropha oil and the right amount of NiW/Ti-USY catalyst were added to the reactor. Hydrogen gas was passed into the reactor after leak detection. After a certain time of the reaction, it was cooled naturally and separated by a centrifuge. Then the liquid product was filtered and sampled using a 0.45 μm organic membrane to extract the product oil.

Composition and relative content of the hydrodeoxygenation liquid products were analyzed by gas chromatography–mass spectrometry (GC–MS) using an Agilent 789A/5975C system. The GC was equipped with an HP-5MS capillary column (30 m × 250 μ m × 0.25 μ m). The injector temperature was set to 503 K with an injection volume of 1.0 μ L and a split ratio of 20:1. High-purity helium was used as the carrier gas. The MS conditions were as follows: ion source temperature 523 K; quadrupole temperature 423 K; transfer line temperature 533 K; electron impact ionization energy 70 eV; mass scan range m/z 20 to 450. The solvent delay time was 2 min. Compound identification was performed by comparing mass spectra with the NIST library, and quantitative analysis was carried out using the area normalization method.

RESULTS AND DISCUSSION

Characterization Results of Catalyst

XRD analysis

Figure 1 shows the XRD of the catalyst with different loads. The XRD curves of b, c, d, e all contained the characteristic diffraction peak of a (USY), indicating that the construction of USY carrier was not significantly changed regardless of the modification of TiO₂ or the load of NiW active components. The anatase phase TiO₂ diffraction peak (PDF # 21-1272) appeared at a 2θ value of 25.3 (101), 37.9 (004), 48.2 (200), 54.5 (105), 62.7 (204), indicating that TiO₂ successfully introduced the surface of the USY carrier. In the XRD diagram of the loaded NiW, no obvious oxide characteristic peaks of Ni and W were found because the loaded metal exhibited high dispersion.

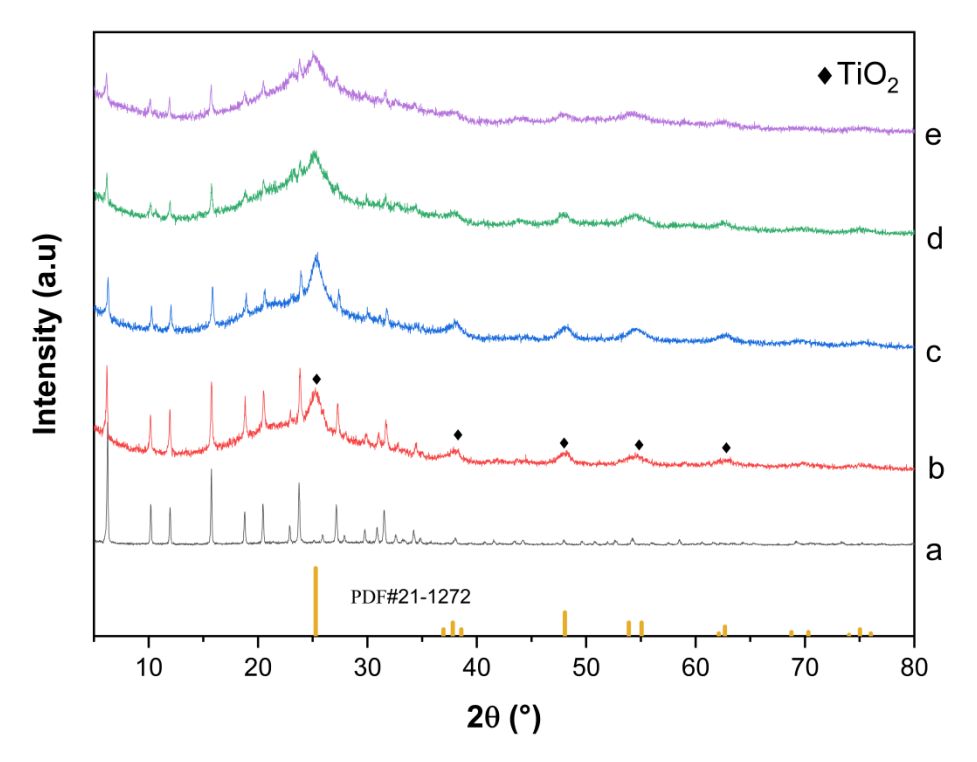


Fig. 1. XRD of NiW/Ti-USY: (a) USY, (b) Ti-USY, (c) 10%NiW/Ti-USY, (d) 20%NiW/Ti-USY, (e) 30%NiW/Ti-USY

XPS analysis

Figure 2a shows the Ni 2p spectrum of 30% NiW/Ti-USY, where the binding energy of Ni 2p3/2 was observed at 852.7 and 856.6 eV.

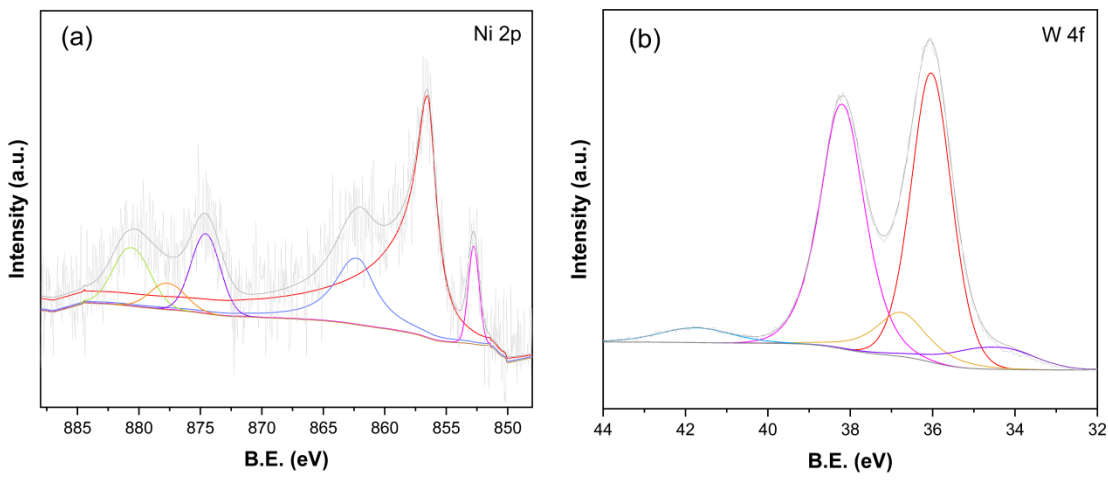


Fig. 2. XPS spectra of 30% NiW/Ti-USY:(a) Ni 2p; (b) W 4f

These characteristic peaks were attributed to Ni⁰ species and Ni²⁺ species, whereas 862.3 and 880.6 eV were attributed to their satellite peaks (Guo *et al.* 2018). According to Fig. 2b, the characteristic peak of the binding energy 36 eV/38.2 eV belongs to the W⁶⁺ (WO₃) species (Xing *et al.* 2020). W⁶⁺ produces oxygen vacancies (Zhang *et al.* 2019) and promotes CO₂ adsorption / activation.

Py-IR analysis

Figure 3 shows the pyridine infrared spectrum of the carrier and 30% NiW/Ti-USY, wherein the Lewis acid and Brønsted acid can be measured by pyridine adsorption. The characteristic peak at 1445 cm⁻¹ demonstrates the Lewis acid site; the characteristic peak at 1488 cm⁻¹ corresponds to adsorption of Brønsted and Lewis acid sites (Chen *et al.* 2022); the characteristic peak at 1541 cm⁻¹ demonstrates the Brønsted acid site (Zhang *et al.* 2021). Table 1 shows the quantitative data table for the acidic sites of USY zeolites at 200 °C and 350 °C. After TiO₂ modification, the levels of Lewis acid and Brønsted acid increased. Both Lewis acid and Brønsted acid were significantly decreased after loading 30% of the active fraction of NiW, probably because NiW interacts with the acidic site on the Ti-USY surface, disrupting a certain number of acidic site structures.

Table 1. Acidity of Catalyst at 200 °C and 350 °C

Catalytic	Acid Density at 200 °C(mmol/g)		Acid Density at 350 °C (mmol/g)	
	Brønsted acid	Lewis acid	Brønsted acid	Lewis acid
USY	0.0781	0.0000	0.0561	0.0000
Ti-USY	0.2066	0.1132	0.1459	0.0693
30%NiW/Ti-USY	0.0138	0.0153	0.0131	0.0089

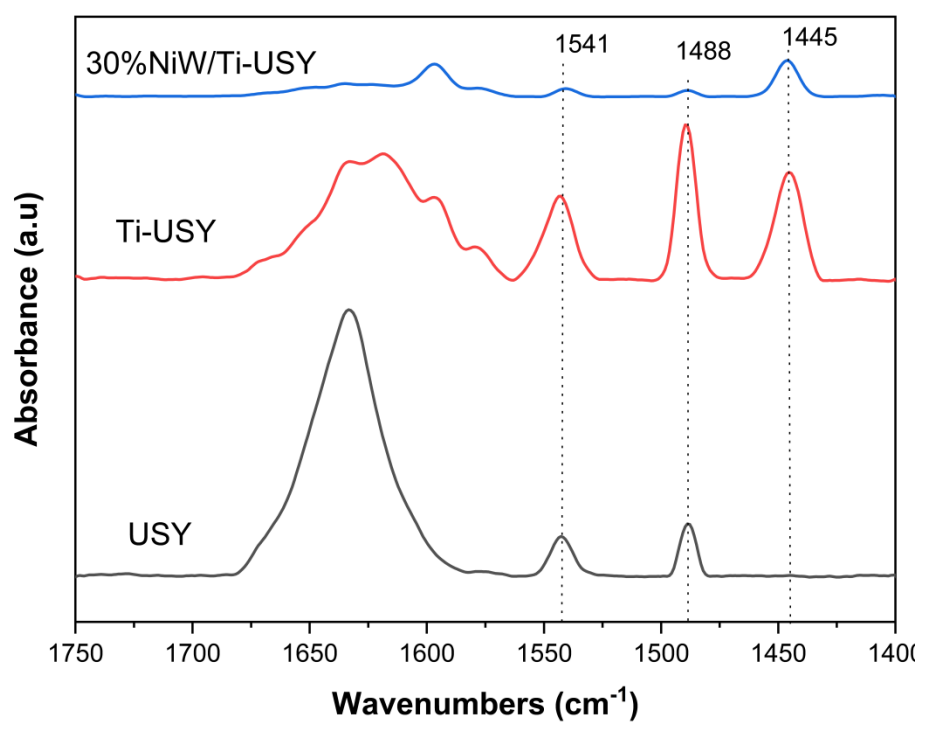


Fig. 3. Py-IR spectra of carrier and 30% NiW/Ti-USY

SEM and TEM analysis

Figure 4 (a) (c) and TEM Figure 5 (a) (c) show that the catalyst surface after loading the metal active component NiW was relatively smooth, but small metal particles were uniform and displayed no obvious agglomeration. Figure 4 (a) (b) (d) and 5 (a) (b) (d) show that after modification, the surface roughness of the catalyst was significantly increased due to the large particle size of TiO₂, and prominent metal particles became evident.

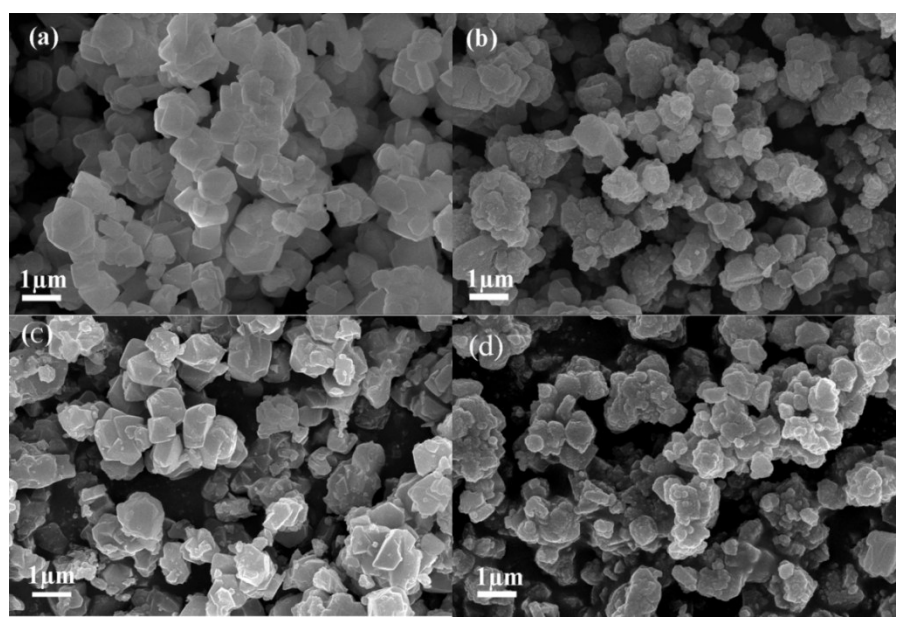


Fig. 4. SEM images of (a) USY, (b) Ti-USY, (c) NiW/USY, and (d) NiW/Ti-USY

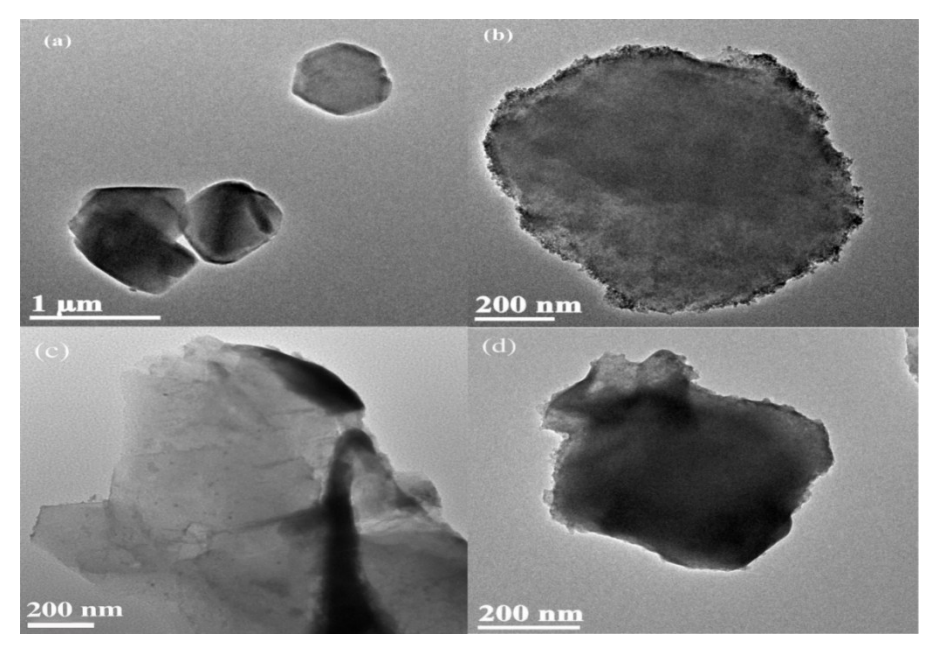


Fig. 5. TEM images of (a) USY, (b) Ti-USY, (c) NiW/USY, and (d) NiW/Ti-USY $BET\ analysis$

Figure 6 shows that all the materials exhibited Type IV isotherms with hysteresis loops, indicating their classification as mesoporous materials. Figure 6f shows the pore size distribution of the five samples, most of which were concentrated around 3 nm, which further shows that all materials were predominantly mesoporous.

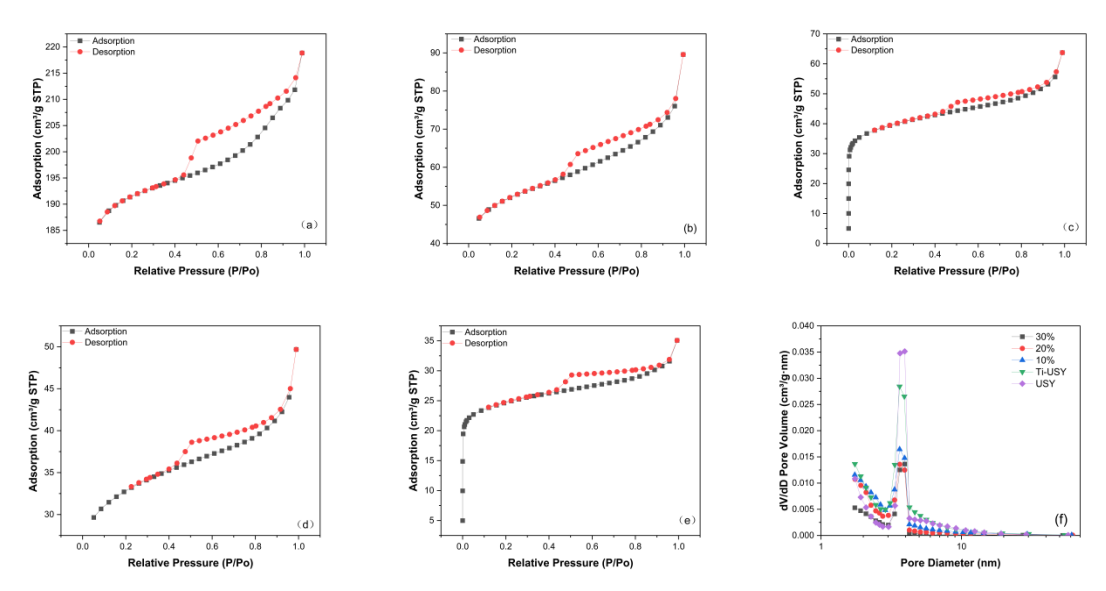


Fig. 6. N₂ adsorption-desorption curves of carriers and catalysts with different NiW loadings, (a) USY,(b) Ti-USY, (c) 10%NiW/Ti-USY, (d) 20%NiW/Ti-USY, (e) 30%NiW/Ti-USY, (f) the distribution of pore size

The textural properties of the catalysts are summarized in Table 2. After loading 30 wt% NiW, the USY support exhibited a significant decrease in both specific surface area and pore volume (SBET: $580 \rightarrow 308 \text{ m}^2/\text{g}$; VBJH: $0.057 \rightarrow 0.033 \text{ cm}^3/\text{g}$), which is mainly attributed to the physical blockage of zeolite channels by metal oxide particles (Hui *et al.*

2019). After Ti modification, the Ti-USY sample showed an increase in pore volume (0.078 cm³/g) compared to the original USY (0.057 cm³/g). It is speculated that this increase resulted from the creation of new pores due to etching during modification or the formation of secondary mesopores through the stacking of TiO₂ particles (Zheng *et al.* 2025).

Table 2. Pore Structure Properties of Supports and Catalysts with Different NiW Loadings

Catalytic	SBET (m²/g)	VBJH (cm³/g)	DBJH (nm)
USY	580	0.057	6.2
30%NiW/USY	308	0.033	6.6
Ti-USY	161	0.078	6.2
10%NiW/Ti-USY	123	0.053	5.6
20%NiW/Ti-USY	104	0.037	5.4
30%NiW/Ti-USY	77	0.023	5.2

However, after further loading the NiW active components onto the Ti-modified support, both the specific surface area and pore volume showed a monotonic decreasing trend (e.g., VBJH decreased from 0.078 cm³/g for Ti-USY to 0.023 cm³/g for 30% NiW/Ti-USY). This indicates that the highly loaded metal particles and Ti species synergistically contribute to pore blockage, collectively occupying the main pore channels of the support and significantly altering the textural properties of the catalyst (Li et al. 2021).

Analysis of Hydrodeoxygenation Properties of Catalyst to Bio-oil

Comparison of the catalytic effect of the catalyst with or without TiO2 modification

Table 3 illustrates the impact of TiO₂ modification on the catalytic performance of jatropha oil. Upon examination of Table 3, it becomes evident that the concentration of oxygenated compounds diminished from 11.6% to 8.3%, while the content of alkenes dropped from 15.7% to 9.6%. Conversely, the proportion of straight-chain alkanes rose from 37.8% to 42.3%. This demonstrates that the modified catalyst support exhibited enhanced hydrogenation and deoxygenation performance due to the presence of additional acidic sites. The increase in cycloalkane content to 9.12% suggests an improvement in cyclization performance. The aromatic content in the product oil remained largely unchanged between the two catalysts, suggesting that both modified and unmodified catalysts had robust aromatization properties. This aromatization might be attributed to the promotion of straight-chain alkane aromatization by the NiW metal and USY zeolite present in the catalysts.

oxygen compound

Catalytic	NiW/Ti-USY	NiW/USY
Cycloalkane	9.12%	5.43%
Cycloalkene	0.74%	0.00%
Alkene	9.64%	15.67%
Aromatic	26.62%	26.72%
straight-chain alkane	42.34%	37.84%
Isoalkane	3.22%	2.34%
Isomeric olefin	0.00%	0.39%

Table 3. Comparison of Catalytic Product Composition between NiW/Ti-USY and NiW/USY

Note: Reaction conditions: 10 g of jatropha oil, temperature 340 °C, hydrogen pressure 1 MPa, catalyst amount 0.5 g, reaction time 4 h

8.33%

Comparison of the catalytic effects of different TiO2 modification amounts

According to Fig. 7 and Table 4, the catalyst performance exhibited a nonlinear variation with increasing Ti modification content. The oxygenate content remained relatively stable as the Ti content increased from 3% to 6% (13.19% \rightarrow 12.86%), but dropped sharply to 8.33% at 9% Ti. This plateau and subsequent decline originated from the complex interplay among acid sites, metal-support interactions, and mass transfer effects.

At moderate Ti loadings (3 to 6%), the newly introduced Lewis acid sites promote C–O bond cleavage, but they also induce side reactions such as coking, leading to the passivation of active sites. Meanwhile, incipient blockage of USY micropores by TiO₂ species hinders reactant diffusion and disrupts the intimacy between metal sites (Ni–W) and acid sites, thereby suppressing the hydrogen spillover effect and stalling deoxygenation efficiency (Wang *et al.* 2020).

A Ti loading of 9% achieved optimal synergy: TiO₂ species provided a suitable number of medium-strength Lewis acid sites that effectively activate C–O bonds, while simultaneously optimizing the anchoring of Ni – W particles, enhancing dispersion and metal-support interaction, and maximizing hydrogen spillover efficiency. This enables immediate hydrogenation of oxygenated intermediates and facilitates the hydrodeoxygenation pathway, as evidenced by the lowest olefin content (9.64%) and the highest selectivity toward linear alkanes (42.34%) (Zhang *et al.* 2022).

At 12% Ti, severe pore blockage (SBET decreased to 52 m²/g) led to significantly hampered mass transfer and a decline in hydrodeoxygenation performance. Simply increasing acid site density is insufficient to ensure high performance; the key lies in achieving an optimal balance of metal-acid synergy (Chen *et al.* 2021). Based on the more pronounced decrease in oxygenate content compared to olefins, it is concluded that acid sites exert a greater influence on catalytic cracking than on catalytic hydrogenation.

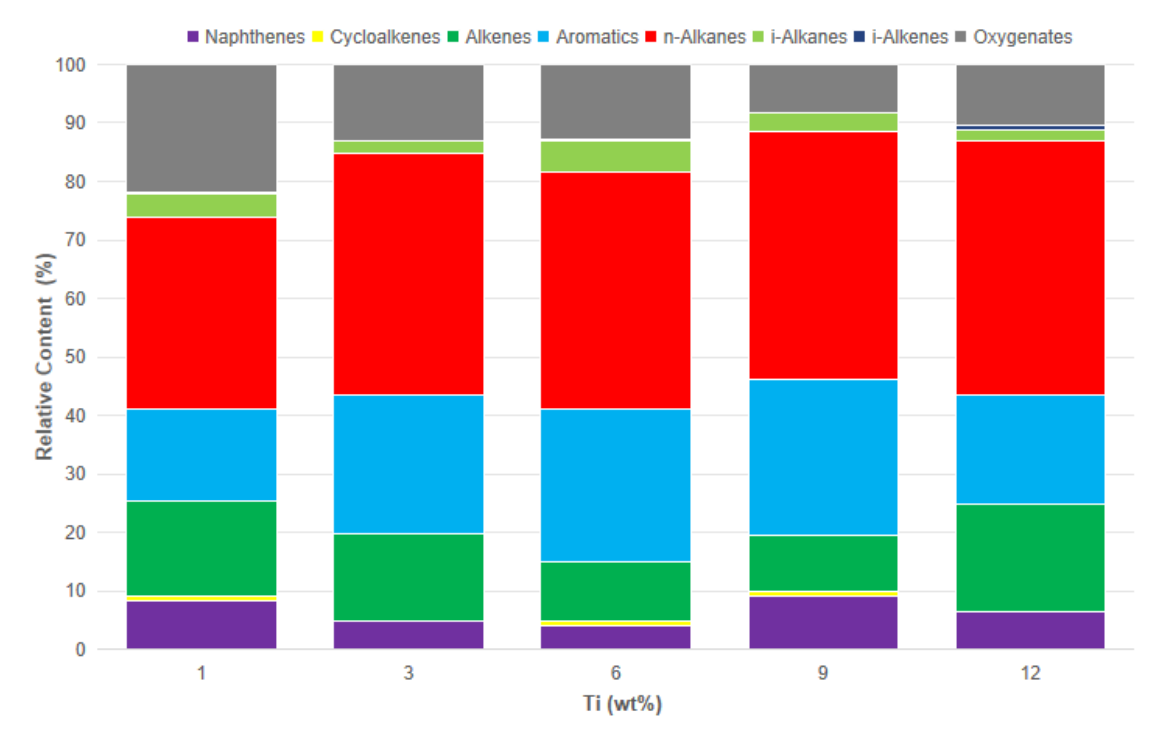


Fig. 7. Hydrodeoxidation of jatropha oil by 30% NiW/Ti-USY catalysts with different Ti modification amounts. Reaction conditions: 10 g of jatropha oil, temperature 340 °C, hydrogen pressure 1 MPa, catalyst amount 0.5 g, reaction time 4 h

Ti content	SBET (m²/g)	VBJH (cm³/g)	DAVE (nm)
1%	559	0.095	2.4
3%	564	0.108	2.4
6%	589	0.091	2.4
9%	161	0.078	2.9
12%	52	0.047	3.9

Table 4. Pore Structure Properties of Carriers with Different Ti Contents

Comparison of the catalytic effects with different NiW ratios

According to Fig. 8, the content of oxygenated compounds was 15.7% and 12.8% respectively, when the active component consisted entirely of Ni or W. Upon achieving a Ni:W ratio of 5:5, the oxygenated compounds content peaked at 20.34%. When the Ni:W ratio was 1:9, the catalyst demonstrated optimal HDO performance, with the oxygenate content decreasing to 7.7% while the selectivity toward n-alkanes reached 36.9%. This phenomenon stems from the synergistic effect of the Ni - W bimetallic active centers: W species are primarily responsible for the activation and cleavage of C–O bonds, whereas Ni species function as hydrogenation sites that promote the hydrogenation saturation of hydrodeoxygenation intermediates (Zhong *et al.* 2019).

In all cases, the relative concentration of alkenes surpassed 20%, and the catalyst hydrogenation was inadequate, which could be attributed to the reaction's low hydrogen pressure of merely 1 MPa or the insufficient loading of active components at just 10%.

The concentration of cycloalkanes exceeded 10%. When the ratio of Ni to W was 1:9, the cycloalkanes achieve a peak concentration of 18.4%, demonstrating that the optimal NiW ratio was conducive to enhancing the cyclization reaction.

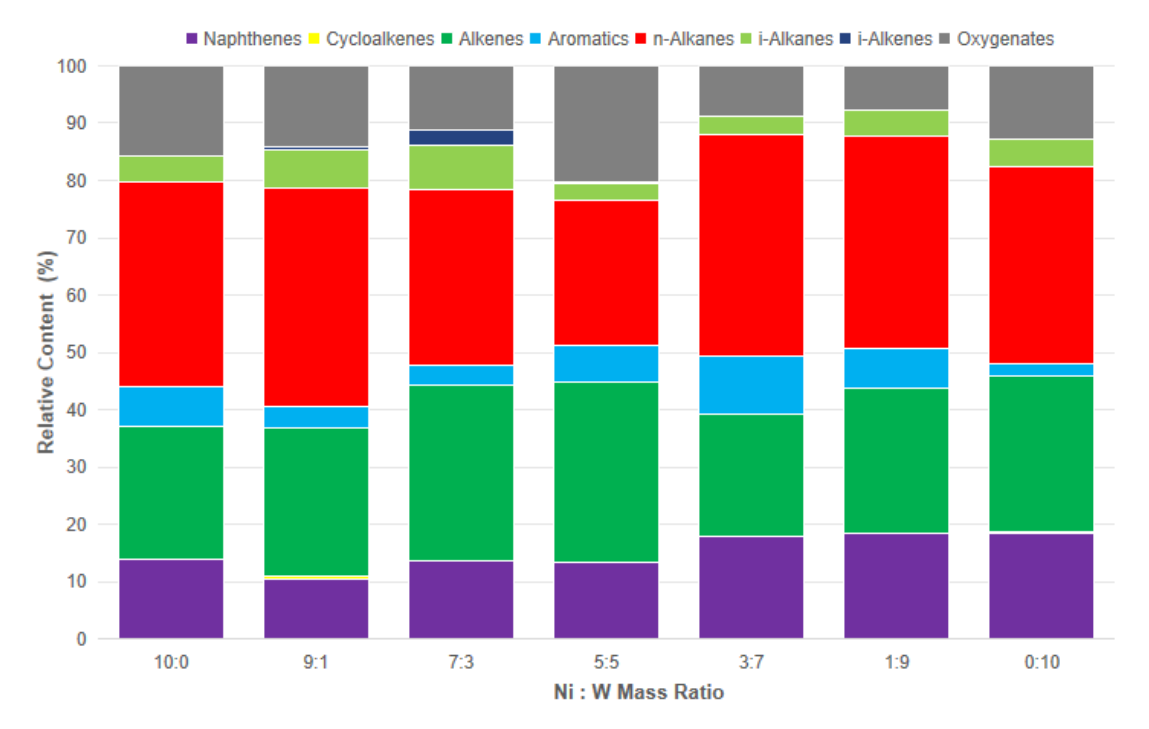


Fig. 8. Hydrodeoxidation of jatropha oil by catalysts with different NiW ratios. Reaction conditions: 10 g of jatropha oil, temperature 340 °C, hydrogen pressure 1 MPa, catalyst amount 0.5 g, reaction time 4 h

Comparison of the catalytic effects of bimetal NiW loading capacity

According to Fig. 9, the metal loading significantly influenced the product distribution of hydrodeoxygenation (HDO). When the loading increased from 10% to 30%, the selectivity toward linear alkanes continuously improved (from 36.9% to 42.3%), indicating that higher metal loading favors the hydrogenation-dominated pathway. The oxygenate content showed a rebound at 20% loading (12.71%) and decreased to the lowest level at 30% loading (8.3%), demonstrating a notable "threshold effect." This trend is closely related to the balance between active site accessibility and mass transfer limitations.

From a reaction mechanism perspective, an adequate amount of NiW active centers (30% loading) provides sufficient bifunctional sites for hydrogenation and deoxygenation. The W⁴⁺/W⁵⁺ redox pairs are responsible for the adsorption and activation of C–O bonds, while the Ni⁰/Ni²⁺ species promote the dissociation of H₂ to generate active hydrogen species, which are subsequently transported to the reaction interface *via* hydrogen spillover effects (Wang *et al.* 2020). The high loading ensures close contact between metallic species, forming an efficient hydrogen transfer network. This facilitates the timely hydrogenation of oxygenated intermediates into alkanes, significantly suppressing the desorption of olefin intermediates (olefin content decreased from 25.3% to 9.6%). Taking into account both oxygenate and olefin contents, the NiW/Ti-USY catalyst with 30% loading exhibited the best hydrodeoxygenation performance.

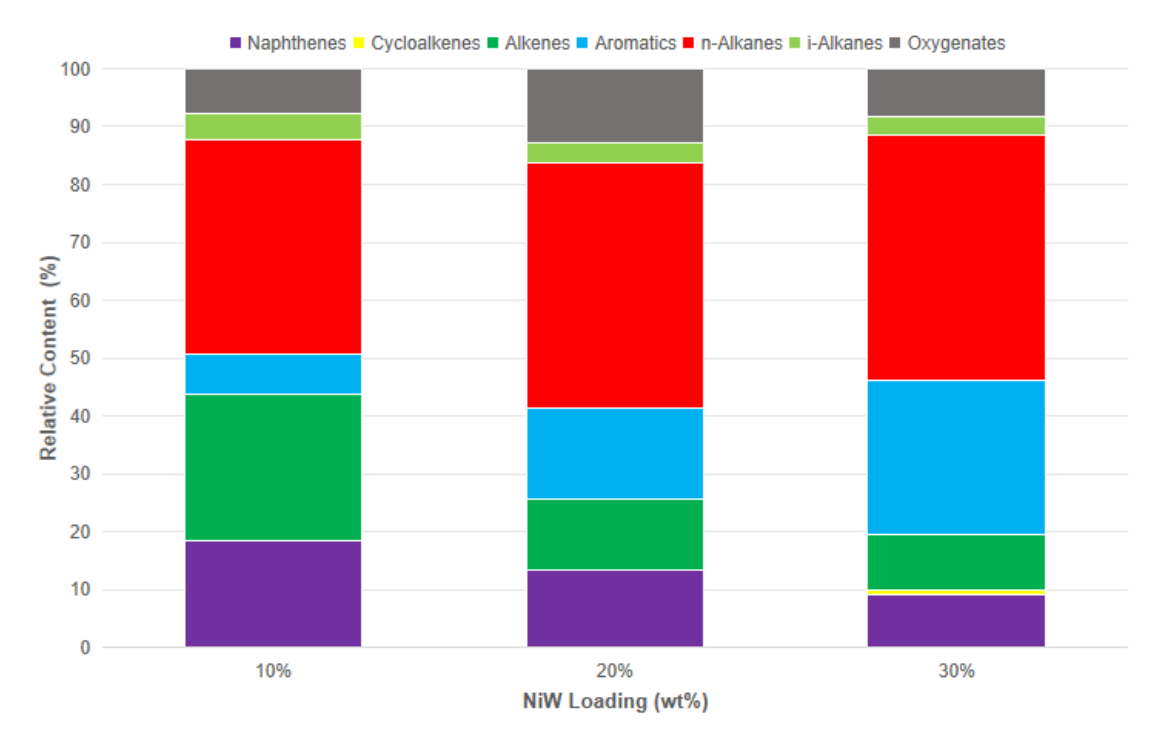


Fig. 9. Catalytic effect of NiW/Ti-USY with different NiW loading. Reaction conditions: 10 g of jatropha oil, temperature 340 °C, hydrogen pressure 1 MPa, catalyst amount 0.5 g, reaction time 4 h

Reaction Mechanism Research

The hydrodeoxygenation (HDO) of Jatropha oil over the NiW/Ti-USY catalyst is synergistically catalyzed by metallic sites and acid sites. The reaction proceeds primarily *via* the decarbonylation/decarboxylation (DCO/DCO₂) pathway, as strongly evidenced by the significantly higher content of C₁₅ and C₁₇ alkanes (30.2%) compared to C₁₆ and C₁₈ alkanes (2%) in Table 5. Meanwhile, the acidity of the catalyst also induces side reactions such as aromatization, cyclization, and isomerization during C–O bond activation, generating considerable amounts of aromatic hydrocarbons (*e.g.*, dodecylbenzene, 7.88%) and naphthenes, thereby reducing the selectivity toward linear alkanes.

Optimization of the catalyst structure revealed that 9% Ti modification optimized the Lewis acidity and enhanced metal-support interaction, promoting hydrogen spillover. A 30% NiW loading ensured sufficient active sites while maintaining pore accessibility, and a Ni:W mass ratio of 1:9 achieved optimal synergy between W species (dominant in deoxygenation) and Ni species (dominant in hydrogenation). Thus, the high performance of this catalyst fundamentally stems from a precise balance between metallic and acidic functions at the nanoscale.

Table 5. Liquid Components of *Jatropha curcas* Oil Hydrodeoxygenation Catalyzed by NiW/Ti-USY with 30% NiW Loading

Molecular Formula	Chemical Compound	Relative Amount (%)
C ₇ H ₁₆	3-Methylhexane	1.14
C ₇ H ₁₄	Methyl cyclohexane	0.48
C ₇ H ₁₂	1-Methylcyclohexene	0.74
C ₇ H ₈	Methyl benzene	1.59
C ₈ H ₁₈	3-Ethylhexane	2.08
C ₈ H ₁₀	Ethylbenzene	1.02
C ₈ H ₁₀	O-xylene	1.30
C ₉ H ₂₀	Nonane	1.63
C ₉ H ₁₂	N-propylene	0.60
C ₉ H ₁₂	2-Ethyltoluene	0.45
C ₁₀ H ₂₀	5-Decane	0.22
C ₉ H ₁₂	1,2,4-Trimethylbenzene	0.23
C ₁₀ H ₂₂	Decane	1.44
C ₁₀ H ₁₂	1-Methylindane	0.49
C ₁₁ H ₂₄	Undecane	1.66
C ₁₀ H ₁₂	2,3-Dihydro-5-methyl-1H indene	2.22
C ₁₁ H ₁₆	Amylbenzene	0.55
C ₁₀ H ₁₂	1,2,3,4-Tetrahydro-naphthalene	0.39
C ₈ H ₁₆ O ₂	Octoic acid	0.26
C ₁₂ H ₂₆	Dodecane	2.33
C ₁₂ H ₁₈	1-Phenylhexane	0.71
C ₁₁ H ₁₄	2,3-Dihydro-4,7-dimethyl-1H indene	0.36
C ₁₁ H ₁₄	6-Methyltetrahydronaphthalene	0.51
C ₁₃ H ₂₈	Tridecane	2.03
C ₁₂ H ₁₆	5-Ethyltetrahydronaphthalene	0.51
C ₁₄ H ₃₀	Tetradecane	1.05
C ₁₅ H ₃₀	Cyclopentadecane	8.64
C ₁₅ H ₃₂	Pentadecane	14.40
C ₁₆ H ₃₂	Hexadecane	2.00
C ₁₇ H ₃₄	Heptadecene	9.42
C ₁₇ H ₃₆	Heptadecane	15.79
C ₁₈ H ₃₈ O	1-Octadecyl alcohol	1.54
C ₁₈ H ₃₀	Dodecylbenzene	7.88
C ₁₈ H ₂₈	1-Octyltetrahydronaphthalene	4.10
C ₁₆ H ₃₂ O ₂	N-Hexadecanoic acid	2.15
C ₁₈ H ₂₈	1-Heptyl-4-methyl-tetrahydronaphthalene	3.71
C ₁₈ H ₃₀ O	Dodecylphenol	4.38

Future Perspectives

Future work should prioritize the evaluation of the catalyst's potential for practical applications, focusing on its durability, poisoning mechanisms, and regenerability. Indepth studies should investigate its deactivation behavior during extended operation, specifically examining the coke deposition rate, location of carbon accumulation, and the extent of metal sintering.

Additionally, it is essential to assess the poisoning effects of common sulfur-, nitrogen-, and phosphorus-containing impurities in feedstock oils on both acidic and metallic sites, and to determine the catalyst's poison tolerance. Developing efficient regeneration strategies—such as controlled calcination to remove coke, replenishment of active metals, or secondary modification to restore deactivated acid sites—is critical to evaluating the catalyst's performance recoverability and cycling stability.

CONCLUSIONS

This study successfully elucidated the structure-activity relationship of the NiW/Ti-USY catalyst in the hydrodeoxygenation (HDO) of jatropha oil through systematic modulation of Ti modification and NiW active phase parameters. The results demonstrated that a Ti mass fraction of 9% represents the optimal threshold for achieving the best performance. At this level, the catalyst maintains a suitable pore structure (SBET = 161 m^2 /g) while forming an optimized distribution of Lewis acid sites and enhanced metal-support interactions.

A Ni/W mass ratio of 1:9 exhibited a significant synergistic effect, wherein W species primarily facilitate C–O bond cleavage, while Ni species promote hydrogenation and hydrogen spillover. A total metal loading of 30% achieved an optimal balance between the quantity and quality of active sites.

Under optimal catalyst conditions, the reaction predominantly proceeded *via* the decarbonylation/decarboxylation pathway, generating C₁₅ and C₁₇ alkanes as the main products. The oxygenate content was reduced to 8.33%, and linear alkane selectivity reached 42.3%. However, the olefin content remained at 9.64%. Overall, the influence of acid sites outweighed that of metal sites in governing the catalytic behavior.

ACKNOWLEDGMENTS

This work was supported by the Projects of Technical Innovation of Hainan Scientific Research Institutes (KYYSGY2023-002) and the Hainan Province's Key Research and Development Project (ZDYF2024GXJS314).

REFERENCES CITED

- Chen, B., Rao, R., Cao, M., He, C., Qian, Y., Qiu, X., and Ouyang, X. (2022). "Mild hydrodeoxygenation of lignin-derived bio-oils to hydrocarbons over bifunctional ZrP₂O₇-Ni₁₂P₅ catalysts," *Fuel* 313(5997). DOI: 10.1016/j.fuel.2021.123044
- Chen, X., and Li, M. (2023). "Hydrodeoxygenation of vegetable oils over Ni-based catalysts supported on modified zeolites," *Bioresource Technology* 387, article 129543. DOI: 10.1016/j.biortech.2023.129543
- Chen, X., Yang, J., Zhang, W., and Li, Y. (2021). "Pore confinement and mass transfer effects in Ti-modified zeolite catalysts for bio-oil upgrading," *Microporous and Mesoporous Materials* 310, article 110634. DOI: 10.1016/j.micromeso.2020.110634
- Fang, Y., Li, W., Wang, Z., and Liu, Y. (2024). "Design of high-performance hydrodeoxygenation catalysts for biomass valorization," *ACS Catalysis* 14(5), 3210-3229. DOI: 10.1021/acscatal.3c05521
- Guo, F., Li, J., Li, W., Chen, X., Qi, H., Wang, X., and Yu, Y. (2018). "Quinoline hydrodenitrogenation over NiW/Al-MCM-41 catalysts with different Al contents," *Russian Journal of Applied Chemistry* 90(12), 2055-2063. DOI: 10.1134/S1070427217120242
- García-Mendoza, S., Ramirez, A., and Fernandez, J. L. (2023). "Stability and deactivation mechanisms in hydrodeoxygenation catalysts: A critical review," *Chemical Engineering Journal* 471, article 144567. DOI:

- 10.1016/j.cej.2023.144567
- Hui, K. S., Duan, X., and Li, M. (2019). "Effect of NiMo loading on the hydrodesulfurization performance of Al₂O₃-based catalysts. *Catalysis Today* 321-322, 99-105. DOI: 10.1016/j.cattod.2018.11.027
- Knothe, G. (2022). "Biodiesel and its properties: Beyond ASTM standards," *Energy and Fuels* 36(3), 1173-1183. DOI: 10.1021/acs.energyfuels.1c03378
- Li, C., Zhang, S., and Wang, T. (2021). "Design of hierarchical ZSM-5 supported NiW catalysts for hydrodeoxygenation of phenolic compounds," *Fuel* 291, 120-135. DOI: 10.1016/j.fuel.2021.120135
- Li, H., Wang, J., and Zhang, K. (2024). "Novel catalyst support materials for enhanced hydrodeoxygenation of biomass-derived oils," *BioResources* 19(2), 1234-1245. DOI: 10.15376/biores.19.2.1234-1245
- Liu, H., Wang, J., Zhang, X., and Zhao, Y. (2024). "Non-precious metal catalysts for hydrodeoxygenation: Recent progress and perspectives," *Journal of Catalysis* 431, 108-123. DOI: 10.1016/j.jcat.2024.02.015
- Liu, Y., and Yang, S. (2023). "Challenges and strategies for the valorization of non-edible plant oils *via* catalytic processes," *BioResources* 18(4), 5678-5692. DOI: 10.15376/biores.18.4.5678-5692
- Wang, J., Xu, Y., Zhang, J., and Zhao, Y. (2020). "Enhanced hydrogen spillover and catalytic activity in hydrodeoxygenation over Ti-modified supported catalysts," *Applied Catalysis B: Environmental* 264, article 118532. DOI: 10.1016/j.apcatb.2019.118532
- Wang, L., and Chen, X. (2024). "Advancements in green diesel production from lignocellulosic biomass and non-edible oils: A technical review," *BioResources* 19(1), 345-357. DOI: 10.15376/biores.19.1.345-357
- Wang, Y., Chen, S., Li, H., and Yang, S. (2023). "Recent advances in catalytic hydrodeoxygenation of biomass-derived oils for renewable diesel production," *Renewable and Sustainable Energy Reviews* 187, article 113756. DOI: 10.1016/j.rser.2023.113756
- Xu, Z., and Cheng, S. (2024). "Zeolite-based catalysts for advanced bio-fuel production: A review," *Microporous and Mesoporous Materials* 365, article 112345. DOI: 10.1016/j.micromeso.2024.112345
- Xing, S., Liu, Y., Liu, X., Li, M., Fu, J., Liu, P., Lv, P., and Wang, Z. (2020). "Solvent-free hydrodeoxygenation of bio-lipids into renewable alkanes over NiW bimetallic catalyst under mild conditions," *Applied Catalysis B-Environmental* 269, article 118718. DOI: 10.1016/j.apcatb.2020.118718
- Zhang, J., Yin, R., Shao, Q., and Zhu, T. (2019). "Oxygen vacancies in amorphous InOx nanoribbons enhance CO₂ adsorption and activation for CO₂ electroreduction," *Angewandte Chemie-International Edition* 58, 5609-5613. DOI: 10.1002/anie.201900167
- Zhang, L., Wang, H., Li, X., and Liu, S. (2022). "Optimal Ti loading in NiW/Ti-USY catalysts for maximizing metal-acid synergy in hydrodeoxygenation," *Chemical Engineering Journal* 428, article 131156. DOI: 10.1016/j.cej.2021.131156
- Zhang, L., Wang, P., and Liu, G. (2022). "Challenges and strategies in the catalytic upgrading of biomass-derived oils: A review," *Fuel Processing Technology* 237, article 107470. DOI: 10.1016/j.fuproc.2022.107470
- Zhang, Y., Liu, T., Xia, Q., and Jia, H. (2021). "Tailoring of surface acidic sites in Co-MoS(2) catalysts for hydrodeoxygenation reaction," *The Journal of Physical*

- Chemistry Letters 12(21), 5668-5674. DOI: 10.1021/acs.jpclett.1c01201
- Zhong, H., Jiang, C., Zhong, X., and Wang, J. (2019). "Non-precious metal catalyst, highly efficient deoxygenation of fatty acids to alkanes, with *in situ* hydrogen from water," *Journal of Cleaner Production* 209, 1228-1234. DOI: 10.1016/j.jclepro.2018.10.318
- Zhong, H., Jiang, C., Zhong, X., and Wang, J. (2023). "Advanced non-precious metal catalysts for efficient deoxygenation of fatty acids to alkanes," *Bioresource Technology* 389, article 129842. DOI: 10.1016/j.biortech.2023.129842
- Zheng, Y., Wang, J., and Liu, C. (2025). "Microstructural regulation and water electrolysis performance of rolled titanium porous transport layers *via* oxalic acid etching," *International Journal of Hydrogen Energy* 50(3), 1234-1245. DOI: 10.1016/j.ijhydene.2024.11.123

Article submitted: May 13, 2025; Peer review completed: June 30, 2025; Revised version received: September 24, 2025; Accepted: September 26, 2025; Published: October 21, 2025.

DOI: 10.15376/biores.20.4.10552-10567